HOKKAIDO UNIVERSITY

Title	Octupole correlations in the excited 0+states and two-neutron transfers in actinide nuclei
Author(s)	Nomura, Kosuke
Citation	Physical Review C, 114(1) https://doi.org/10.1103/8ff2-58j6
Issue Date	2026-07-06
Doc URL	https://hdl.handle.net/2115/100292
Rights	©2026 American Physical Society
Type	journal article
File Information	v3.pdf

Hokkaido University Collection of Scholarly and Academic Papers : HUSCAP

Octupole correlations in the excited 0^+ states and two-neutron transfers in actinide nuclei

Kosuke Nomura*
Department of Physics, Hokkaido University, Sapporo 060-0810, Japan and
Nuclear Reaction Data Center, Hokkaido University, Sapporo 060-0810, Japan
(Dated: June 19, 2026)

Impacts of octupole correlations on low-energy excited 0^+ states and two-neutron transfer intensities in Ra and Th isotopes are analyzed within the interacting boson model, using the Hamiltonian parameters that are obtained from the microscopic nuclear density functional theory calculations. Incorporating the octupole degree of freedom in the model is shown to give an overall reasonable description of the ground-state-band energy levels and to lower the 0^+_2 ones significantly. The calculation yields a number of excited 0^+ states, most of which are formed by the configurations of more than one octupole bosons. Octupole correlations make significant contributions to the $0^+_1 \to 0^+_2$ (p,t) and (t,p) transfer intensities in those nuclei in which the octupole collectivity is most enhanced. Behaviors of the predicted transfer intensities with the increasing neutron number along the isotopic chain reflect nuclear structural evolution.

I. INTRODUCTION

The intrinsic shape of the atomic nucleus is characterized mostly by the quadrupole deformations [1]. A higher-order deformation of octupole type comes into play in low-lying states in those nuclei with specific neutron N and/or proton Z numbers, e.g., 34, 56, 88, 134, for which a $\Delta j = \Delta l = 3$ coupling of the single-particle orbits is possible [2–6]. Evidence for the permanent octupole deformation was found in a few radioactive nuclei, e.g., ^{220}Rn and ^{224}Ra [7], which exhibit a negative-parity, $K^\pi = 0^-_1$, band close in energy to the ground-state, $K^\pi = 0^+_1$, band; they form an approximate alternating-parity band that is connected by strong electric dipole ($E1$) and octupole ($E3$) transitions. While the static octupole shape rarely occurs in real nuclei, the octupole degree of freedom and its coupling to the quadrupole degree of freedom are important building blocks to describe low-energy nuclear structure.

One of the peculiar features of the nuclear structure is the presence of low-energy excited 0^+ states and corresponding bands, which have been observed in many nuclei. These excited 0^+ energy levels often exhibit a parabolic behavior with N in a given isotopic chain, being particularly low near the middle of the major shell. These characteristics point to the coexistence of multiple intrinsic shapes [8–12], considered nowadays to be a universal phenomenon that is found in a wide range of the nuclear chart. In the rare-earth region, the lowering pattern of the 0^+ energy levels has also been identified as a signature of the quantum phase transitions (QPTs) in nuclear shapes [13–16]. Alternative interpretation has been provided in terms of the pairing vibrations [17–25]. Nuclei in rare-earth and actinide regions with $(N,Z) \approx (88,56)$ and $(134,88)$, respectively, are characterized by the pronounced octupole collectivity. The low-energy 0^+ states observed in these regions have been suggested to be of two-octupole-phonon nature [4]. Related experiments were performed, e.g., by means of the two-neutron transfer reactions [1, 21] for actinide [26–30] and rare-earth [31–36] nuclei. The interpretation of the low-energy 0^+ states and the corresponding $K^\pi = 0^+$ bands remains an open problem, and it would be of interest to give an appropriate theoretical description of these phenomena, that is based on a certain microscopic nuclear structure.

The present study aims to address the octupole correlation effects on the ground and excited 0^+ states and two-neutron transfer reactions in actinides, using the interacting boson model (IBM) [37]. The IBM comprises as basic building blocks correlated monopole and quadrupole pairs of valence nucleons, which are approximated by s and d bosons, respectively. It has been successful in describing low-energy quadrupole collective states in medium-heavy and heavy nuclei, and was also applied to compute (p,t) and (t,p) transfer intensities as signatures of the QPTs [38–42]. In a recent study [43], octupole correlation effects on the excited 0^+ states and two-neutron transfer reactions in Nd, Sm, and Gd isotopes near the shape transition point, $N \approx 90$, were studied using the IBM that includes the octupole, f, boson degree of freedom, using the Hamiltonian parameters derived by means of the self-consistent mean-field (SCMF) method in the framework of the nuclear density functional theory (DFT) [44–47]. This version of the IBM, denoted hereafter mapped IBM, has been successfully used in nuclear structure studies (see Ref. [48] for a review and references therein). The *sdf*-IBM calculations in Ref. [43] produced a number of excited 0^+ states that consist of the configurations of more than one f bosons, and produced QPT-like behaviors of the $0^+ \to 0^+$ (p,t) and (t,p) transfer intensities as functions of N.

The present study extends the analysis of Ref. [43] to the even-even actinide, Ra and Th nuclei, in which enhanced octupole collectivity is expected. Previous DFT-mapped IBM studies [49–51] suggested an occurrence of octupole shape phase transitions in Th and Ra isotopes,

* nomura@sci.hokudai.ac.jp

that is, transitions from nearly spherical to stable octupole and to octupole-soft shapes. In these studies, while the main focus was placed on the properties of the yrast states, possible double-octupole-phonon nature of the 0_2^+ states was also pointed out in a few selected nuclei. The scope of the present study is to provide a more systematic investigation of the relevance of the octupole collectivity in the 0^+ states in Ra and Th. As compared with the rare-earth nuclei, experimental information of the two-neutron transfers in actinide region is rather scarce. The IBM calculations with the s, d, f, and p (or dipole) boson degrees of freedom were made to interpret (p,t) data for a few nuclei, ^{228}Th [26, 28], ^{230}Th [26, 27], ^{232}U [26], and ^{240}Pu [29, 30], in which parameters of the *spdf*-IBM were fitted to experimental low-energy spectra. Predictions of the (p,t) and (t,p) transfer intensities are here made within the mapped IBM, which is guided by the self-consistent calculations within the nuclear DFT. In particular, spectroscopic properties of the Ra and Th nuclei considered in the present work were studied in the previous mapped IBM calculation in Ref. [51], with the microscopic input being provided by the Hartree-Fock-Bogoliubov (HFB) [47] self-consistent calculations using the D1M parametrization [52] of the Gogny force [53]. The derived values of the IBM parameters in Ref. [51] are employed in the present work.

In Sec. II, a brief description of the theoretical framework to compute the two-nucleon transfers is given. Calculated low-energy spectra, transition properties, (p,t) and (t,p) transfer intensities are presented in Sec. III. A summary of main results is provided in Sec. IV.

II. THEORETICAL PROCEDURE

The collective quadrupole and octupole states are described in terms of the s, d, and f boson degrees of freedom [37, 54–57], which represent collective 0^+, 2^+, and 3^- pairs of valence nucleons, respectively [37, 58, 59]. The present version of the IBM does not distinguish like-proton from like-neutron bosons, and is referred to as *sdf*-IBM-1, which is hereafter denoted *sdf*-IBM unless otherwise specified. The number of bosons, denoted $N_{\rm B}$, is equal to that of pairs of valence nucleons, and is constant for a given nucleus.

The *sdf*-IBM Hamiltonian adopted in this study is of the form

$$\hat{H}_{\rm B} = \epsilon_d \hat{n}_d + \epsilon_f \hat{n}_f + \kappa_2 \hat{Q}_2 \cdot \hat{Q}_2 + \kappa_3 \hat{Q}_3 \cdot \hat{Q}_3 + \rho \hat{L}_d \cdot \hat{L}_d \ . \tag{1}$$

The first and second terms, respectively, denote the d-boson and f-boson number operators, defined as $\hat{n}_d = d^\dagger \cdot \tilde{d}$ and $\hat{n}_f = f^\dagger \cdot \tilde{f}$, with ϵ_d and ϵ_f being the single d-boson and f-boson energies relative to that of s bosons. Note that $\tilde{d}_\mu = (-1)^{-\mu} d_{-\mu}$ and $\tilde{f}_\mu = (-1)^{3-\mu} f_{-\mu}$. The third and fourth terms represent the quadrupole-quadrupole and octupole-octupole interactions with strengths κ_2 and κ_3, respectively. The last term concerns the corrections to the rotational bands. The corresponding boson operators are defined as

$$\hat{Q}_2 = s^\dagger \times \tilde{d} + d^\dagger \times \tilde{s} + \chi_d (d^\dagger \times \tilde{d})^{(2)} + \chi_f (f^\dagger \times \tilde{f})^{(2)} \tag{2a}$$

$$\hat{Q}_3 = s^\dagger \times \tilde{f} + f^\dagger \times \tilde{s} + \chi_3 (d^\dagger \times \tilde{f} + f^\dagger \times \tilde{d})^{(3)} \tag{2b}$$

$$\hat{L}_d = \sqrt{10} (d^\dagger \times \tilde{d})^{(1)} \ . \tag{2c}$$

The use of the Hamiltonian of the form (1) is inspired by the earlier microscopic IBM study of Ref. [57], in which the *sdf*-IBM-1 Hamiltonian similar to (1) was derived from a proton-neutron octupole-octupole boson interaction by mapping the totally-symmetric state in the proton-neutron *sdf*-IBM onto the corresponding IBM-1 state. The same form of the *sdf*-IBM Hamiltonian as in (1) was used in Ref. [60] for studying quadrupole-octupole collective states in Sm and Gd isotopes.

The parameters of $\hat{H}_{\rm B}$ are derived by associating the *sdf*-IBM Hamiltonian to the SCMF potential energy surface (PES) obtained from the axial quadrupole, β_{20}, and octupole, β_{30}, constrained Gogny-HFB calculations, with β_{20} and β_{30} representing intrinsic deformations related to the axial quadrupole and octupole moments, respectively. The intrinsic properties of a given nucleus is inferred in the *sdf*-IBM from the consideration of the boson coherent state,

$$|\phi\rangle = (N_{\rm B}!)^{-1/2} (\lambda^\dagger)^{N_{\rm B}} |0\rangle \tag{3}$$

with

$$\lambda^\dagger = s^\dagger + \tilde{\beta}_{20} d_0^\dagger + \tilde{\beta}_{30} f_0^\dagger \ . \tag{4}$$

$\tilde{\beta}_{\lambda 0}$ are bosonic quadrupole and octupole deformations, and are assumed to be proportional to the fermionic intrinsic deformations as $\tilde{\beta}_{\lambda 0} = C_\lambda \beta_{\lambda 0}$, with C_λ being the constants of proportionality [49, 61]. Taking the expectation value of $\hat{H}_{\rm B}$ in the coherent state $|\phi\rangle$ gives rise to the energy surface in the *sdf*-boson system. The *sdf*-IBM PES, $E_{\rm IBM}(\beta_{20}, \beta_{30})$, is then associated with that calculated within the constrained Gogny-HFB method, $E_{\rm HFB}(\beta_{20}, \beta_{30})$, so that an approximate relation

$$E_{\rm IBM}(\beta_{20}, \beta_{30}) \approx E_{\rm HFB}(\beta_{20}, \beta_{30}) \tag{5}$$

should hold in the vicinity of the equilibrium minimum of the PES. The strength ρ for the $\hat{L}_d \cdot \hat{L}_d$ term is obtained independently of the above PES-mapping procedure so that [62] the bosonic cranking moment of inertia [63] at the equilibrium point along the $\beta_{30} = 0$ axis should be equal to the HFB counterpart computed by the Thouless-Valatin formula [64]. The details of the *sdf*-IBM mapping procedure and the adopted values of the parameters are found in Ref. [51]. Note that the ϵ_f energies used in Ref. [51] are here modified, because the $\hat{L}_f \cdot \hat{L}_f$ term, with $\hat{L}_f = \sqrt{28} (f^\dagger \times \tilde{f})^{(1)}$, was contained in the Hamiltonian in Ref. [51], but is not in the present work. The mapped *sdf*-IBM Hamiltonian is diagonalized in the boson m-scheme basis [65], providing excitation energies and wave functions.

The (p,t) and (t,p) transfer strengths are computed as

$$I^{(p,t)}(0_i^+ \to 0_f^+) = |\langle N-2, 0_f^+ | \hat{P}^{(p,t)} | N, 0_i^+ \rangle|^2 \quad (6)$$

$$I^{(t,p)}(0_i^+ \to 0_f^+) = |\langle N+2, 0_f^+ | \hat{P}^{(t,p)} | N, 0_i^+ \rangle|^2 . \quad (7)$$

$|N, 0_i^+\rangle$ and $|N \mp 2, 0_f^+\rangle$ stand for the *sdf*-IBM wave functions for the 0^+ states in an initial and a final nuclei with N and $N \mp 2$ in the (p,t) and (t,p) reactions, respectively. $\hat{P}^{(p,t)}$ and $\hat{P}^{(t,p)}$ are bosonic (p,t) and (t,p) transfer operators and are expressed as

$$\hat{P}^{(p,t)} = c_1 \left[\hat{A}(\Omega_\nu, N_\nu)\tilde{s} + c_2 \hat{n}_f \tilde{s} \right] \quad (8)$$

and

$$\hat{P}^{(t,p)} = c_1 \left[s^\dagger \hat{A}(\Omega_\nu, N_\nu) + c_2 s^\dagger \hat{n}_f \right] , \quad (9)$$

respectively, where $\hat{P}^{(t,p)} = \left(\hat{P}^{(p,t)}\right)^\dagger$, and c_1 and c_2 are parameters. The operator $\hat{A}(\Omega_\nu, N_\nu)$ is defined as [38]

$$\hat{A}(\Omega_\nu, N_\nu) = \left(\Omega_\nu - N_\nu - \frac{N_\nu}{N_\mathrm{B}} \hat{n}_d \right)^{1/2} \left(\frac{N_\nu + 1}{N_\mathrm{B} + 1} \right)^{1/2} , \quad (10)$$

where Ω_ν denotes the degeneracy of the neutron pairs in a given major shell, and is equal to $(184-126)/2 = 29$ for the actinide nuclei under consideration. N_ν stands for the number of like-neutron bosons, i.e., $N_\nu = 1$, 2, ..., 12 for those even-even nuclei with $N = 130$, 132, ..., 150, respectively. As in literature [37], the operator $\hat{n}_d$ in Eq. (10) is replaced with its expectation value in the ground state of the initial nucleus, i.e., $\langle 0_{1,i}^+ | \hat{n}_d | 0_{1,i}^+ \rangle$.

The operators similar to those in (8) and (9) were frequently used in the phenomenological *spdf*-IBM calculations for two-neutron transfers in actinides [26–30], in which in addition to the $s(^\dagger)\hat{n}_f$ term the term that involves p boson operator, $s(^\dagger)\hat{n}_p$, was considered. It was also shown that for the descriptions of the two-nucleon transfers contributions from the negative-parity bosons were essential. The first terms in the operators in (8) and (9), $\hat{A}(\Omega_\nu, N_\nu)s(^\dagger)$, in fact, arise from the seniority consideration within the *sd*-IBM [38], while the second terms, $s(^\dagger)\hat{n}_f$, are specific terms involved in more general transfer operators in the *sdf*-IBM and the addition of these terms to $\hat{A}(\Omega_\nu, N_\nu)s(^\dagger)$ may not be fully justified from a microscopic point of view. However, the use of these specific forms, (8) and (9), are just adequate for the present purpose, which is to study the impacts of the octupole degree of freedom on the transfer strengths.

In addition, to analyze the f-boson effects on spectroscopic properties quantitatively, the *sd*-IBM mapping calculations are also performed, with the maximum number of f bosons being set to be zero. The corresponding transfer operators in the *sd*-boson model thus consist only of the first terms in (8) and (9).

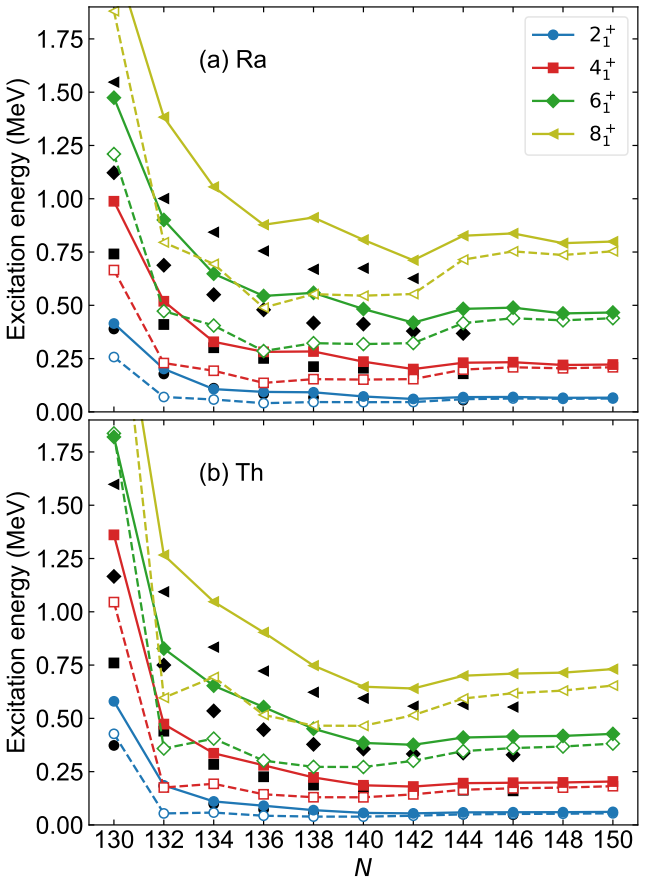

FIG. 1. Energy spectra of even-spin positive-parity yrast states in Ra and Th isotopes calculated with the mapped *sdf*-IBM and *sd*-IBM, represented by the solid and open symbols connected by the solid and dashed lines, respectively. The experimental data are adopted from Ref. [66], and are shown as the black solid symbols.

III. RESULTS

A. Low-energy structure

Figures 1 and 2 present, respectively, the energy spectra of even-spin positive-parity yrast states in the ground-state ($K^\pi = 0_1^+$) band, obtained from the *sdf*-IBM and *sd*-IBM, and the those of odd-spin negative-parity yrast states, which are considered as the members of the $K^\pi = 0_1^-$ band. The *sdf*-IBM results for the excitation energies for these yrast states are also given in Fig. 4 of Ref. [51]. The differences from the previous calculation of Ref. [51] are that, due to the neglect of the $\hat{L}_f \cdot \hat{L}_f$ term in the present calculation, the $K^\pi = 0_1^+$ band is here stretched, while $K^\pi = 0_1^-$ band levels are systematically lowered; for example, the 2_1^+ energy levels are raised by $\approx 10 \sim 30$ %, and the 1_1^- bandhead of the $K = 0_1^-$ band is lowered by $\approx 50 \sim 150$ keV; the differences are most significant for nuclei with $N \approx 136$. These changes, how-

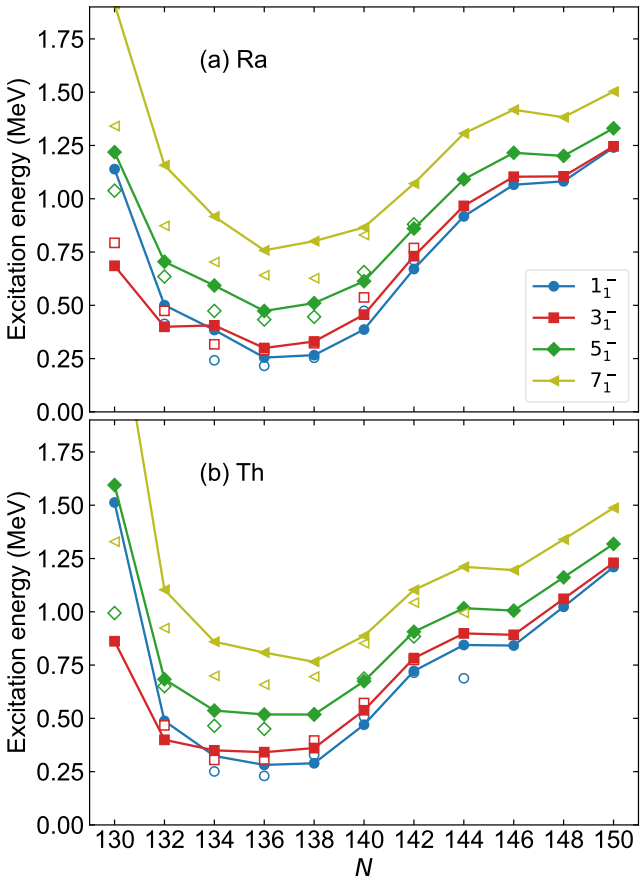

FIG. 2. Energy spectra for the odd-spin negative-parity yrast states obtained from the mapped *sdf*-IBM, represented by the solid symbols connected by the solid lines. Experimental data, adopted from Ref. [66], are depicted as open symbols.

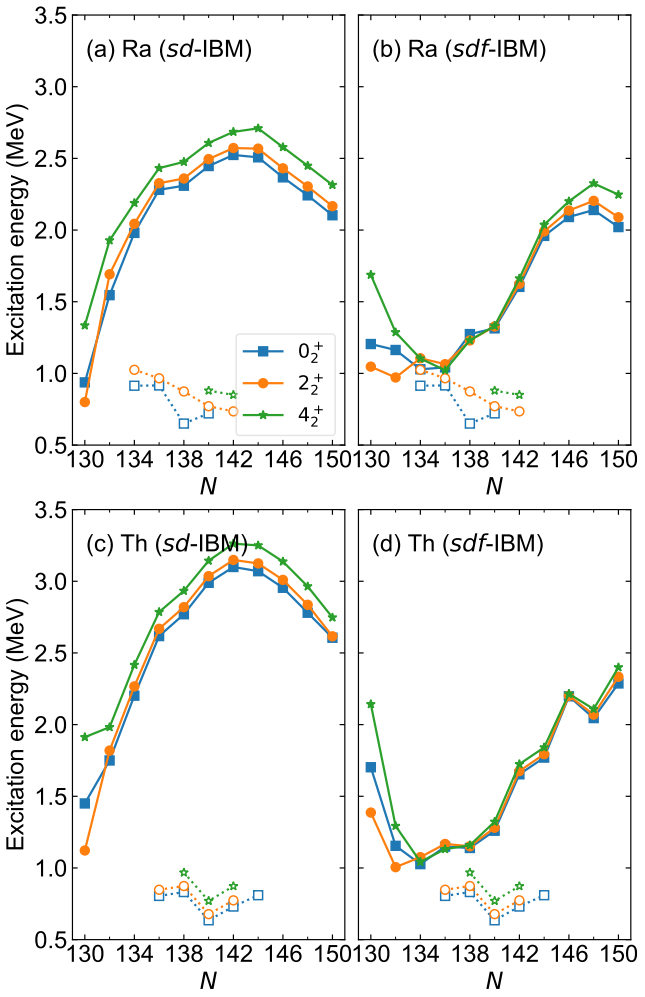

FIG. 3. Predicted excitation energies of nonyrast states, 0_2^+, 2_2^+, and 4_2^+, within the *sd*-IBM [(a) and (c)] and *sdf*-IBM [(b) and (d)], represented by the solid symbols connected by the solid lines. The corresponding experimental data, adopted from Ref. [66], are depicted as open symbols connected by dotted lines.

ever, do not alter major conclusions on the properties of these yrast states.

From Fig. 1, in general, the *sd*-IBM considerably underestimates the experimental data, while the *sdf*-IBM energy spectra are higher than those from the *sd*-IBM and are more consistent with the data. Pronounced differences between the two IBM predictions are apparent near $N = 132$. This implies that the octupole degree of freedom plays a part in the positive-parity yrast states within the mapped *sdf*-IBM. The negative-parity energy levels, shown in Fig. 2, exhibit a parabolic behavior as functions of N, being minimal at $N \approx 136$. The Gogny-HFB SCMF calculations [51] suggested for many of the Ra and Th nuclei an octupole-deformed ground state at $(\beta_{20}, \beta_{30}) \approx (0.14, 0.11)$, $(0.16, 0.13)$, $(0.18, 0.14)$, $(0.20, 0.12)$, and $(0.22, 0.09)$ for $^{220-228}$Ra, respectively, and at $(\beta_{20}, \beta_{30}) \approx (0.14, 0.11)$, $(0.16, 0.13)$, $(0.20, 0.16)$, and $(0.22, 0.16)$ for $^{222-228}$Th, respectively. One can see that the largest octupole deformation is suggested at $N \approx 136$, i.e., ^{224}Ra in the Ra chain and ^{226,228}Th in the Th chain. The $K = 0_1^\pm$ bands obtained for these nuclei were shown to form an approximate alternating parity band [51], while for $N > 138$ the predicted $K = 0_1^-$ band increases in energy and is decoupled from the $K = 0_1^+$ one. This structural change can be a signature of the transition from the stable octupole deformed to octupole-soft shape phase transition; for further details, see Refs. [50, 51].

The octupole degree of freedom has significant influences on the nonyrast states, as illustrated in Fig. 3. The *sd*-IBM considerably overestimates the observed 0_2^+, 2_2^+, and 4_2^+ energy levels, which exhibit an inverse parabola. In the *sdf*-IBM, however, these energy levels rather show a parabolic systematic, being lowest in energy at $N = 136$ (for Ra) and $N = 134$ (for Th); this systematic is qualitatively consistent with the observed one [66], apart from the fact that the lowest-energy 0_2^+ levels are ex-

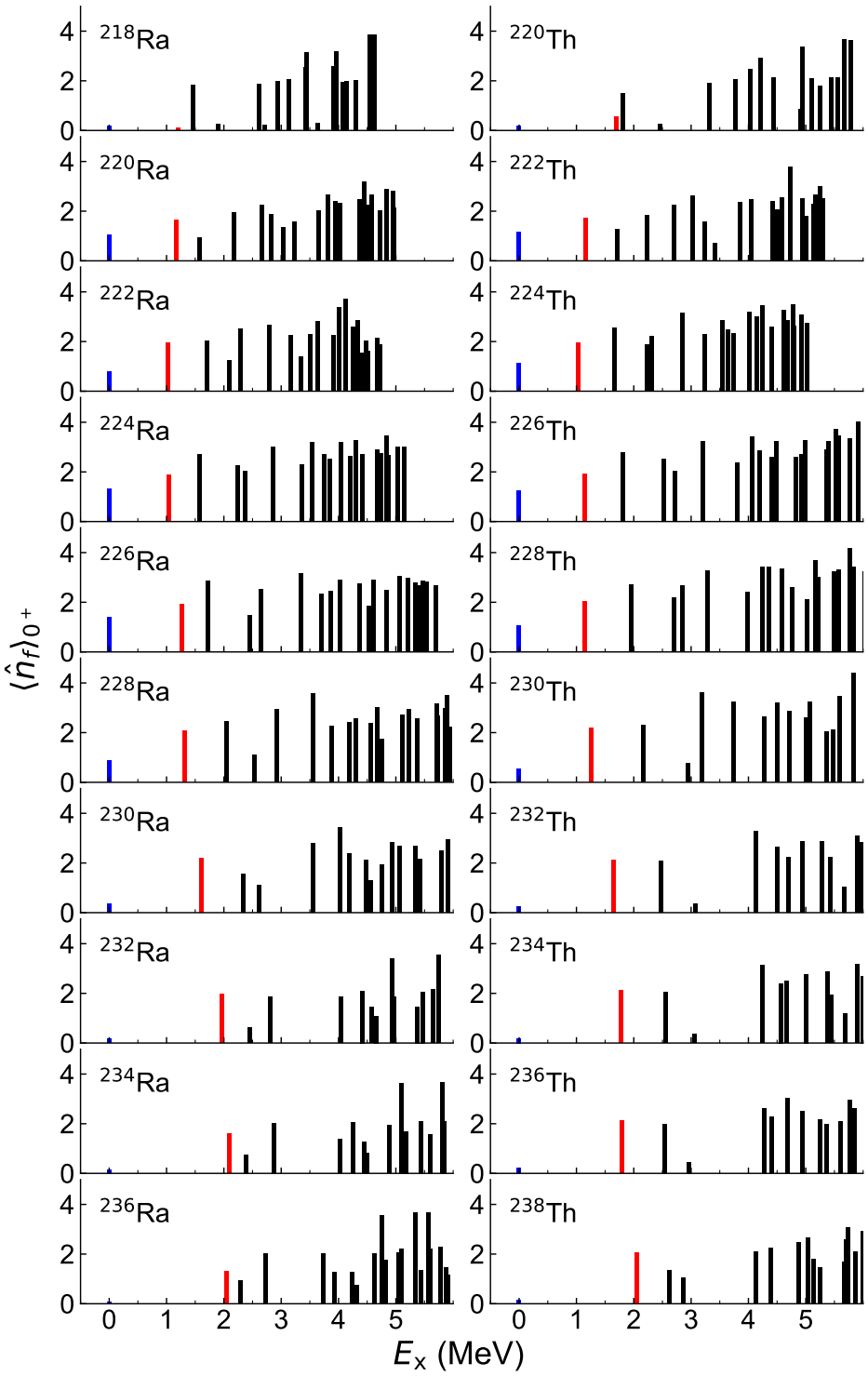

FIG. 4. Expectation values of the f-boson number operator, $\langle \hat{n}_f \rangle_{0_n^+}$ ($n \geqslant 1$), in the 0_n^+ states in Ra and Th isotopes, plotted against the corresponding energies, $E_{\rm x}$. The $\langle \hat{n}_f \rangle_{0_1^+}$ and $\langle \hat{n}_f \rangle_{0_2^+}$ values are highlighted in color blue and red, respectively.

perimentally found at $N = 138$ (Ra) or 140 (Th). Most significant quantitative differences between the *sdf*-IBM and *sd*-IBM predictions are observed in isotopes with $N \leqslant 142$, in which octupole correlations are expected to be particularly enhanced. For $N > 142$, there is no notable difference in the calculated 0_2^+, 2_2^+, and 4_2^+ exci-

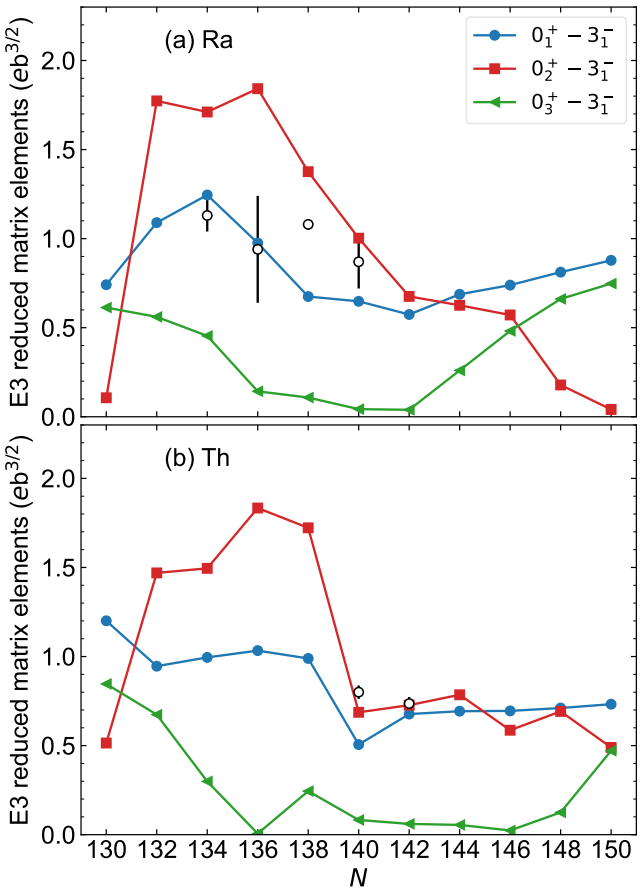

FIG. 5. Absolute values of the calculated reduced matrix elements $|\langle 3_1^- \| \hat{T}(E3) \| 0_1^+ \rangle|$, $|\langle 3_1^- \| \hat{T}(E3) \| 0_2^+ \rangle|$, and $|\langle 3_1^- \| \hat{T}(E3) \| 0_3^+ \rangle|$ in $eb^{3/2}$ units. Experimental $|\langle 3_1^- \| \hat{T}(E3) \| 0_1^+ \rangle|$ values for ^{222,228}Ra [67], ^{224}Ra [7], ^{226}Ra [68], ^{230}Th [69], and ^{232}Th [70] are represented by open circles.

tation energies between the two boson models, indicating that the octupole bosons play a less significant part in these nuclei.

Specifically for ^{222}Ra, ^{224}Ra, ^{226}Th, and ^{228}Th, the mapped *sdf*-IBM reproduces the observed nonyrast levels rather well. This is in a marked contrast with the previous mapped *sdf*-IBM results for the rare-earth nuclei [43], which significantly overestimated the experimental 0_2^+ energy levels. In the mapped IBM calculations in general, the overestimates of the 0_2^+ energy levels are a consequence of the unexpectedly large quadrupole-quadrupole strength. This is largely accounted for by incorporating mixing of normal and intruder configurations in the IBM [71–73]. It has been indeed pointed out that the configuration mixing of different intrinsic shapes and shape coexistence are crucial to interpret the low-energy excited 0_2^+ states in the rare-earth nuclei [74–76]. In the actinide nuclei, the octupole degree of freedom may seem to play a more important role to construct the 0_2^+ states than in the case of the rare-earth nuclei. However, the possibility that certain shape configuration mixing occurs in the actinide nuclei should not be ruled out, given the considerable overestimates of the 0_2^+ levels in ^{226,228}Ra and $^{230-234}$Th.

In addition, the 0_2^+, 2_2^+, and 4_2^+ states can be considered to be members of the $K^\pi = 0_2^+$ band. Some traces of such $K^\pi = 0_2^+$ bands are indeed experimentally suggested in several actinide nuclei [66]. As one can see in Fig. 3, the present *sdf*-IBM calculation suggests that these energy levels are lying quite close in energy, more or less consistently with experiment. In some nuclei, however, the *sdf*-IBM does not give correct order of these energy levels, whereas the *sd*-IBM significantly overestimates, but reproduce order of these levels. These predicted nonyrast states in the *sdf*-IBM also exhibit highly complicated $E2$ transition patterns, and it is therefore not straightforward to establish a clear band structure of the excited $K^\pi = 0^+$ bands within the *sdf*-IBM.

The nature of the 0^+ states can be inferred from the calculated expectation values, $\langle 0_n^+ | \hat{n}_f | 0_n^+ \rangle \equiv \langle \hat{n}_f \rangle_{0_n^+}$, in the corresponding *sdf*-IBM wave functions, which provide approximate f-boson content in a given state. Figure 4 displays the $\langle \hat{n}_f \rangle_{0_n^+}$ values for those 0^+ states in Ra and Th nuclei obtained in the *sdf*-IBM with the corresponding excitation energies, E_x, below 6 MeV. Notably, the 0_1^+ ground state of the nuclei $^{220-228}$Ra and $^{222-228}$Th, in particular, contains rather large amounts of the f boson components, $\langle \hat{n}_f \rangle_{0_1^+} \approx 1$, compared with the previous mapped *sdf*-IBM results for Gd, Sm, and Nd isotopes [43], $\langle \hat{n}_f \rangle_{0_1^+} \approx 0.5$. The result shown in Fig. 4 confirms the importance of the octupole correlations to construct the 0_1^+ ground state in those actinide nuclei near $N = 134$, and suggests that the octupole effects in the actinide region are more significant than in the rare-earth region within the mapped IBM. As for the 0_2^+ state, for almost all nuclei studied here, the values $\langle \hat{n}_f \rangle_{0_2^+} \approx 2$ are obtained, indicating the two-octupole-boson structure. A similar conclusion about the 0_2^+ states was reached for the rare-earth nuclei [43, 60].

In deformed rare-earth nuclei, such as some Gd ones, a number of low-energy excited 0^+ states are observed experimentally below 3 MeV, and were considered to arise from the mixture of the octupole-boson configurations in the corresponding 0^+ wave functions in the *sdf*-IBM [31]. The situation may be similar to the actinide region. Indeed, Fig. 4 suggests that in most nuclei many 0^+ states are obtained at higher energies above ≈ 3 MeV, which are composed of approximately two or more f-boson contents. It should be also noted that the relevant experimental information of the nonyrast 0^+ states, which would support the above finding, is rather scarce in the actinide region.

$E3$ transition properties could be another observable signature of the possible double-octupole-phonon nature of the excited 0^+ states. Figure 5 gives the predicted $E3$ reduced matrix elements between the 3_1^- state and lowest

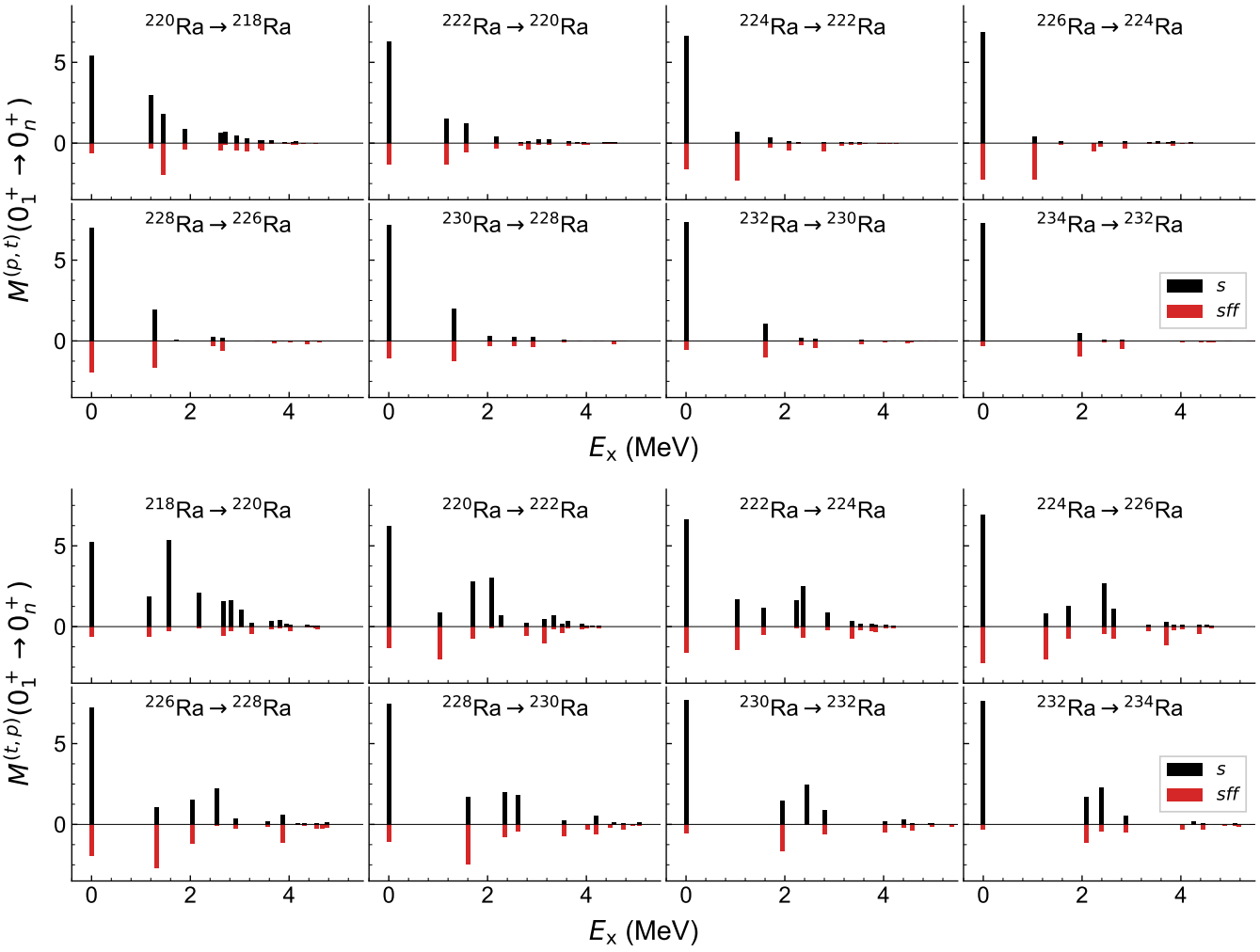

FIG. 6. Calculated matrix elements, (11)–(14) with $n \geqslant 1$, for the $^{A+2}$Ra$(p,t)^{A}$Ra (upper) and ^{A}Ra$(t,p)^{A+2}$Ra (lower) reactions with $A = 218 - 232$, plotted against the excitation energies E_x in the final nucleus. In each plot, the absolute values of the s-boson contributions, $|M_s^{(p,t)}(0_1^+ \to 0_n^+)|$ and $|M_s^{(t,p)}(0_1^+ \to 0_n^+)|$ (denoted "s"), are shown, while the f-boson contributions are shown with their sign being negative, that is, $-|M_{sff}^{(p,t)}(0_1^+ \to 0_n^+)|$ and $-|M_{sff}^{(t,p)}(0_1^+ \to 0_n^+)|$ (denoted "sff").

three 0^+ states, $|\langle 3_1^- \| \hat{T}(E3) \| 0_1^+ \rangle|$, $|\langle 3_1^- \| \hat{T}(E3) \| 0_2^+ \rangle|$, and $|\langle 3_1^- \| \hat{T}(E3) \| 0_3^+ \rangle|$. The $\hat{T}(E3)$ transition operator is given as $\hat{T}(E3) = e_3 \hat{Q}_3$, with e_3 and $\hat{Q}_3$ being the boson effective charge and octupole operator of (2b), respectively. As is conventional, the same value of the parameters χ_3 as that used in the Hamiltonian is employed. In Ref. [51], the e_3 charges that depend on the boson number and on the β_{20} and β_{30} deformations were considered [see Eq. (15) of [51]] in order to incorporate the octupole effects for those nuclei near $N = 134$ and to better reproduce the empirical inverse parabolic systematic of the $B(E3; 3_1^- \to 0_1^+)$ values. These e_3 values are adopted in the present work, which are shown in Fig. 3 of Ref. [51]. From Fig. 5 one sees that the calculated $|\langle 3_1^- \| \hat{T}(E3) \| 0_2^+ \rangle|$ matrix elements are larger than the $|\langle 3_1^- \| \hat{T}(E3) \| 0_1^+ \rangle|$ ones for the nuclei with $N = 132 - 140$. This indicates a strong coupling between the 0_2^+ state and octupole state 3_1^-. Note that the predicted $|\langle 3_1^- \| \hat{T}(E3) \| 0_1^+ \rangle|$ values are overall consistent with the experimental counterparts [7, 67–70].

B. Two-neutron transfers

To study octupole effects on two-nucleon transfers, the following quantities are considered:

$$M_s^{(p,t)}(0_1^+ \to 0_n^+) = \langle N-2, 0_n^+ | \hat{A}(\Omega_\nu, N_\nu) \tilde{s} | N, 0_1^+ \rangle \quad (11)$$

$$M_{sff}^{(p,t)}(0_1^+ \to 0_n^+) = \langle N-2, 0_n^+ | \hat{n}_f \tilde{s} | N, 0_1^+ \rangle \quad (12)$$

$$M_s^{(t,p)}(0_1^+ \to 0_n^+) = \langle N+2, 0_n^+ | s^\dagger \hat{A}(\Omega_\nu, N_\nu) | N, 0_1^+ \rangle \quad (13)$$

$$M_{sff}^{(t,p)}(0_1^+ \to 0_n^+) = \langle N+2, 0_n^+ | s^\dagger \hat{n}_f | N, 0_1^+ \rangle \ . \quad (14)$$

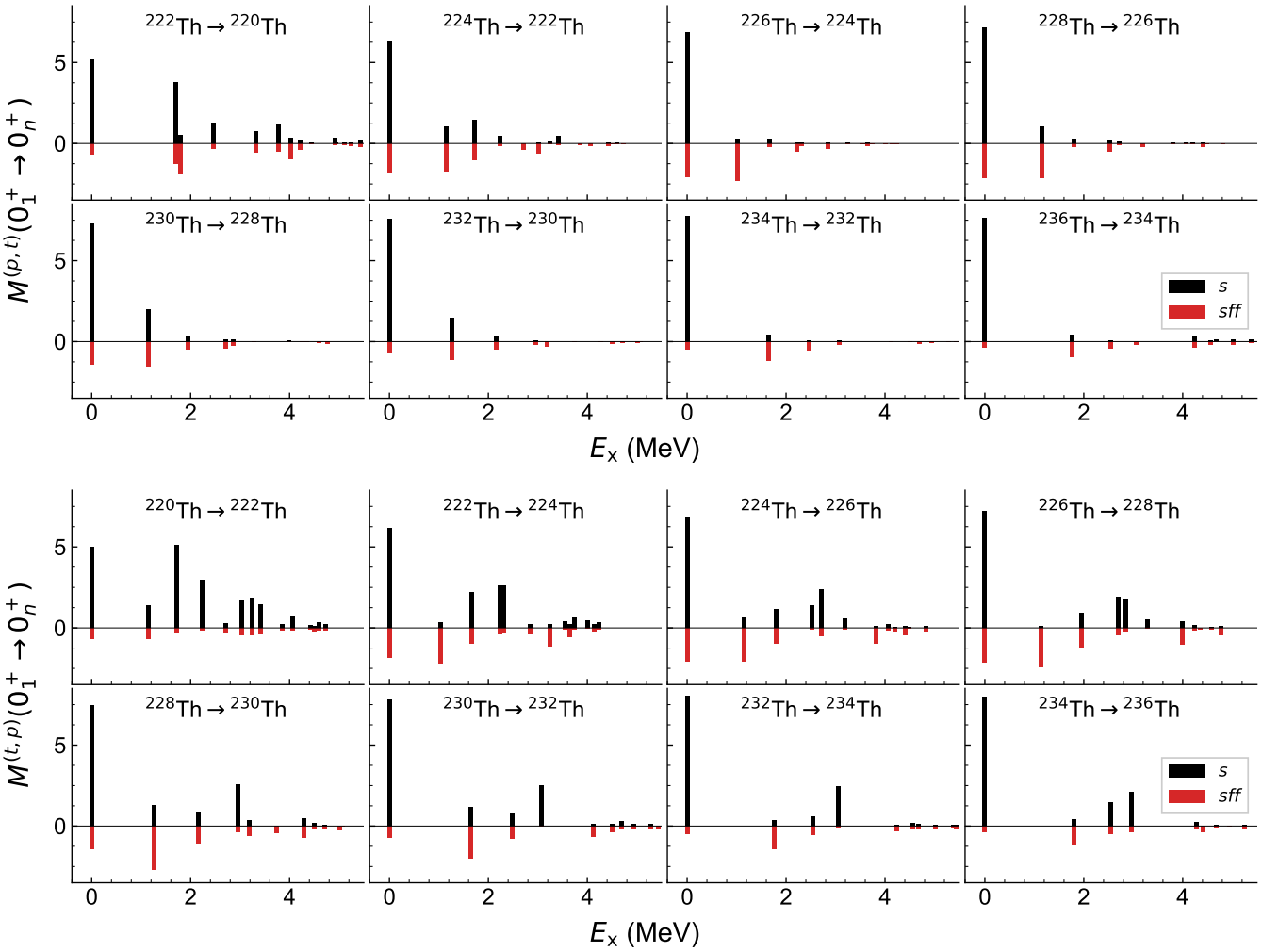

FIG. 7. Same as the caption to Fig. 6, but for the $^{A+2}$Th$(p,t)^{A}$Th (upper) and ^{A}Th$(t,p)^{A+2}$Th (lower) reactions with $A = 220 - 234$.

The matrix element in the first (third) of the above equations corresponds to the first term in Eq. (8) [(9)], while the one in the second (fourth) of the above equations to the second term of (8) [(9)]. In the following, the terms $\hat{A}(\Omega_\nu, N_\nu)s(^\dagger)$ and $s(^\dagger)\hat{n}_f$ are simply referred to as "s-boson" and "f-boson" terms, respectively, and the matrix elements given in (11)–(14) represent their contributions to the transfer intensities. Figures 6 and 7 show the calculated values of the above matrix elements for the $^{A+2}$Ra$(p,t)^{A}$Ra and ^{A}Ra$(t,p)^{A+2}$Ra (with $A = 218 - 234$), and for the $^{A+2}$Th$(p,t)^{A}$Th and ^{A}Th$(t,p)^{A+2}$Th (with $A = 220 - 236$) transfer reactions, respectively.

It is seen from Fig. 6 that, for each of the transfer reactions of Ra, the s-boson contributions to the ground-state-to-ground-state ($0_1^+ \to 0_1^+$) transfers, i.e., $M_s^{(p,t)}(0_1^+ \to 0_1^+)$ and $M_s^{(t,p)}(0_1^+ \to 0_1^+)$, are dominant over the ground-state-to-excited-0$^+$-state ($0_1^+ \to 0_{\rm ex}^+$) ones, $M_s^{(p,t)}(0_1^+ \to 0_n^+)$ and $M_s^{(t,p)}(0_1^+ \to 0_n^+)$ with $n > 1$, in the considered energy range $E_{\rm x} < 5$ MeV. For each transfer reaction, the $M_s^{(p,t)}(0_1^+ \to 0_n^+)$ and $M_s^{(t,p)}(0_1^+ \to 0_n^+)$ values become smaller for higher $E_{\rm x}$. An exception is the ^{218}Ra$(t,p)^{220}$Ra transfer, for which the predicted matrix element $M_s^{(t,p)}(0_1^+ \to 0_3^+)$ is particularly large, being comparable to the $M_s^{(t,p)}(0_1^+ \to 0_1^+)$ value. Both the $M_s^{(p,t)}(0_1^+ \to 0_1^+)$ and $M_s^{(t,p)}(0_1^+ \to 0_1^+)$ matrix elements become monotonously larger for those transfer reactions of heavier Ra isotopes. As for the $0_1^+ \to 0_1^+$ transfers, the s-boson contributions, $M_s^{(p,t)}(0_1^+ \to 0_1^+)$ and $M_s^{(t,p)}(0_1^+ \to 0_1^+)$, are also considerably larger in magnitude than those of the f-boson term, $M_{sff}^{(p,t)}(0_1^+ \to 0_1^+)$ and $M_{sff}^{(t,p)}(0_1^+ \to 0_1^+)$. In some cases, such as ^{226}Ra$(p,t)^{224}$Ra and ^{224}Ra$(t,p)^{226}$Ra, for which octupole correlations are particularly strong in the initial and final nuclei, the f-boson contributions, represented by the

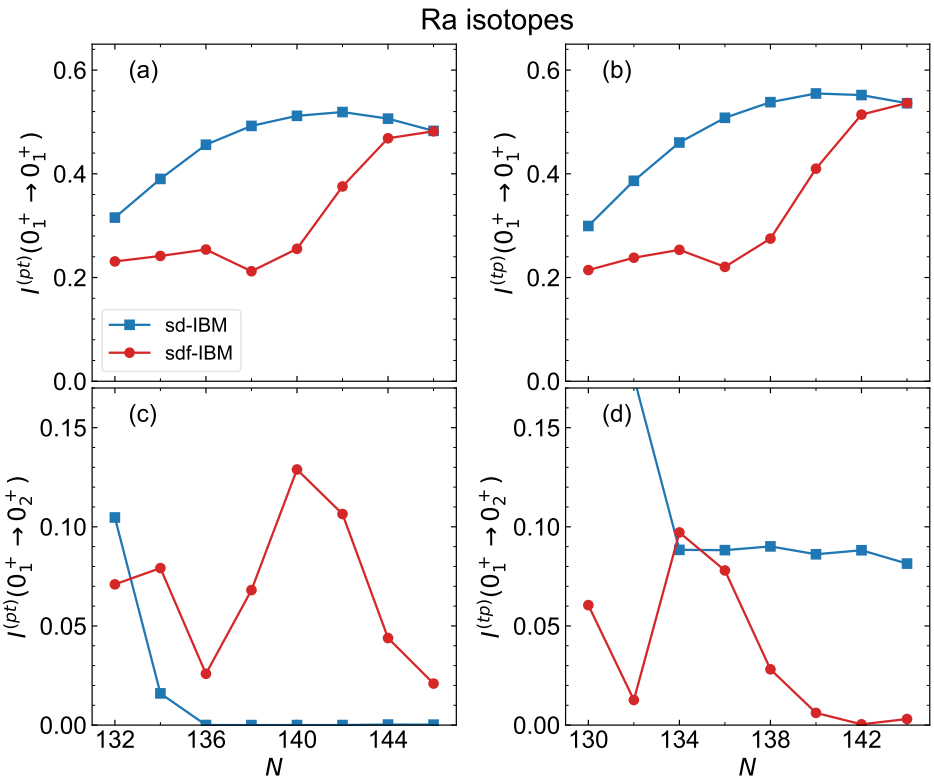

FIG. 8. (p,t) and (t,p) transfer intensities in Ra isotopes depicted as functions of N of the initial nucleus. Results obtained from the mapped *sdf*-IBM are compared with those from the *sd*-IBM.

$M_{sff}^{(p,t)}(0_1^+ \to 0_1^+)$ and $M_{sff}^{(t,p)}(0_1^+ \to 0_1^+)$ matrix elements, are also large. The octupole effects on the $0_1^+ \to 0_1^+$ (p,t) and (t,p) intensities are shown to become minor for the transfer reactions of those nuclei with N that are away from $N \approx 134$.

One can observe from Fig. 6 that the octupole degree of freedom plays particularly important roles in the $0_1^+ \to 0_2^+$ strengths. The $M_{sff}^{(p,t)}(0_1^+ \to 0_2^+)$ and $M_{sff}^{(t,p)}(0_1^+ \to 0_2^+)$ values are calculated to be, in almost all cases, of the same order of magnitude as or even larger in magnitude than the s-boson contributions, $M_s^{(p,t)}(0_1^+ \to 0_2^+)$ and $M_s^{(t,p)}(0_1^+ \to 0_2^+)$. For the transfer strengths to higher-lying nonyrast 0^+ states, $M_{sff}^{(p,t)}(0_1^+ \to 0_n^+)$ and $M_{sff}^{(t,p)}(0_1^+ \to 0_n^+)$ are of the same order of magnitude as $M_s^{(p,t)}(0_1^+ \to 0_n^+)$ and $M_s^{(t,p)}(0_1^+ \to 0_n^+)$, but all these quantities become negligibly smaller for larger E_x.

Similar results are obtained for Th isotopes, which are given in Fig. 7. Apart from some quantitative differences between the results for the Ra and Th isotopic chains, one can thus draw similar conclusions concerning the roles played by the f-boson term and overall systematic of the transfer intensities, both as functions of N along the isotopic chain and of E_x for a given transfer reaction.

The total transfer intensities, $I^{(p,t)}(0_1^+ \to 0_n^+)$ (6) and $I^{(t,p)}(0_1^+ \to 0_n^+)$ (7), are expected to show characteristic behaviors as functions of N, and can be thus identified as a signature of possible QPTs. Experimental observables that can be compared with the predicted transfer intensities are the cross sections measured at particular scattering angles. For the considered Ra and Th isotopes, however, experimental (p,t) and (t,p) data, which could be used to constrain the c_1 and c_2 parameters in the transfer operators, are rather scarce. For this reason, the constant values, $c_1 = 0.1$ and $c_2 = 1$, are employed for all the transfer reactions throughout. In the previous mapped *sdf*-IBM study of the two-neutron transfers in rare-earth nuclei [43], the boson-number and deformation dependent c_2 parameter was proposed. In the phenomenological *spdf*-IBM calculations [29, 30] constant parameters for the term involving negative-parity bosons in the transfer operators were considered.

The $I^{(p,t)}(0_1^+ \to 0_{1,2}^+)$ and $I^{(t,p)}(0_1^+ \to 0_{1,2}^+)$ intensities calculated by the mapped *sdf*-IBM are depicted in Figs. 8 and 9. One can observe, in Figs. 8(a) and 8(b), that the $I^{(p,t)}(0_1^+ \to 0_1^+)$ and $I^{(t,p)}(0_1^+ \to 0_1^+)$ values for the Ra isotopes resulting from the mapped *sdf*-IBM decrease from $N = 136$ to 138 and from $N = 134$ to 136, respectively. The *sd*-IBM counterparts exhibit less significant variation with N. From a group-theoretical point of view, in the limit of large boson number ($N_B \to \infty$) in the *sd*-IBM, the matrix element

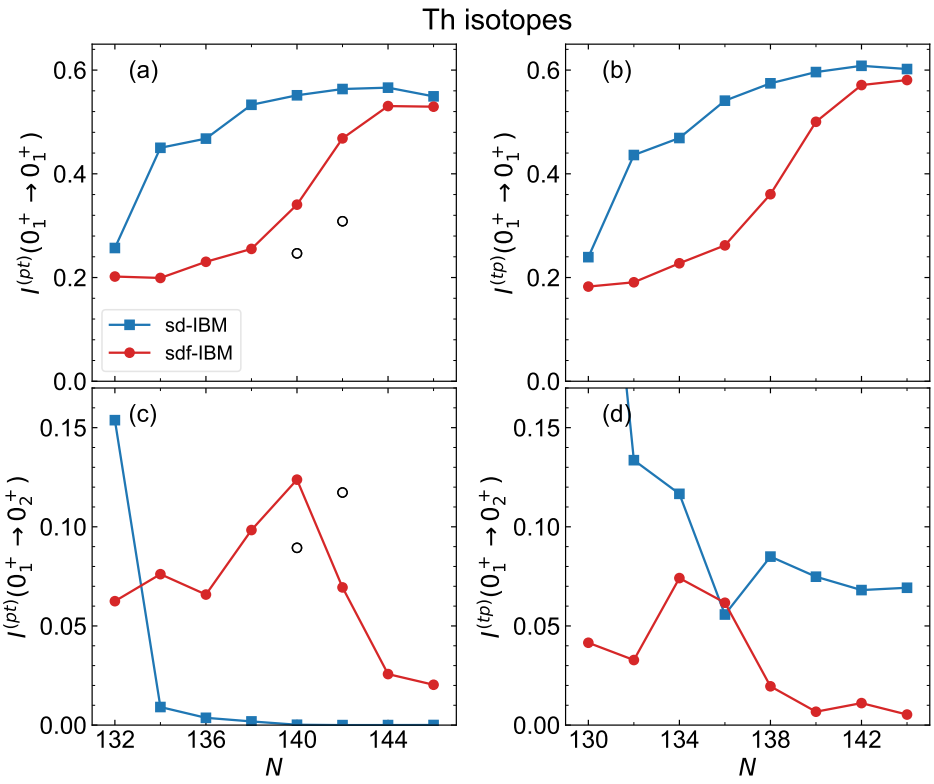

FIG. 9. Same as the caption to Fig. 8, but for the Th isotopes. Experimental data for the ^{230}Th$(p,t)^{228}$Th and ^{232}Th$(p,t)^{230}$Th, adopted from Ref. [26], are differential cross sections in μb/sr units measured at the laboratory angle of 7.5°.

$|\langle N_B+1, 0_1^+|s^\dagger|N_B, 0_1^+\rangle|^2$ is proportional to N_B+1 and $(N_B+1)(2N_B+3)/3(2N_B+1)$ in the U(5) and SU(3) dynamical symmetry limits, respectively [38]. Along the U(5)-SU(3) phase-transition chain, such as those observed in rare-earth nuclei, the $M_s^{(p,t)}(0_1^+ \to 0_1^+)$ value is thus expected to increase in nearly spherical region, decrease suddenly near the critical point, $N = 90$, and start to increase for deformed region, $N > 90$. Since the present IBM involves f bosons, the comparison with the symmetry argument within the *sd*-IBM should be considered to be approximate. Nevertheless, the $I^{(p,t)}(0_1^+ \to 0_1^+)$ and $I^{(t,p)}(0_1^+ \to 0_1^+)$ values resulting from the mapped *sdf*-IBM do exhibit certain traces of possible shape phase transitions in actinides, to which octupole correlations should make substantial contributions.

The $I^{(p,t)}(0_1^+ \to 0_2^+)$ and $I^{(t,p)}(0_1^+ \to 0_2^+)$ transfer intensities, which are shown in Figs. 8(c) and 8(d), also exhibit strong N dependence in the mapped *sdf*-IBM. In particular, they become maximal at $N = 140$ [for (p,t)] and $N = 134$ [for (t,p)], reflecting, to a certain extent, the lowering pattern of the energy levels of the 0_2^+ states, which are shown to be made mainly of the two-f-boson configurations (see Fig. 4). In the *sd*-IBM with $N_B \to \infty$ [38], the $0_1^+ \to 0_2^+$ (p,t) transfer is not allowed in both the U(5) and SU(3) limits; the mapped *sd*-IBM values in Fig. 8(c) follow this in $N > 134$, whereas the *sdf*-IBM gives finite values. The $0_1^+ \to 0_2^+$ (t,p) transfer is allowed in the SU(3) limit, but is not in the U(5) limit; both boson models in the present study provide nonzero $I^{(t,p)}(0_1^+ \to 0_2^+)$ intensities. The previous IBM mapping calculations for the rare-earth Gd, Sm, and Nd isotopes [43] gave similar $I^{(p,t)}(0_1^+ \to 0_2^+)$ and $I^{(t,p)}(0_1^+ \to 0_2^+)$ systematic.

The calculated $I^{(p,t)}(0_1^+ \to 0_{1,2}^+)$ and $I^{(t,p)}(0_1^+ \to 0_{1,2}^+)$ for the Th isotopes are shown in Fig. 9. The *sdf*-IBM values of $I^{(p,t)}(0_1^+ \to 0_1^+)$ and $I^{(t,p)}(0_1^+ \to 0_1^+)$ only monotonously increase with N, hence do not appear to exhibit a QPT-like behavior as the one observed in the Ra isotopes. This can be partly accounted for by the adopted value of the parameter, $c_2 = 1$, which may not be appropriate for Th. In fact it is confirmed that increasing slightly the c_2 value to, e.g., $c_2 \approx 1.5$, leads to similar $I^{(p,t)}(0_1^+ \to 0_1^+)$ and $I^{(t,p)}(0_1^+ \to 0_1^+)$ systematic as that obtained for the Ra isotopes. In Figs. 9(a) and 9(c), experimental data for the ^{230}Th$(p,t)^{228}$Th and ^{232}Th$(p,t)^{230}$Th transfer reactions, adopted from Ref. [26], are shown. These data are measured cross sections at the laboratory angle 7.5°, estimated from the distorted-wave Born approximation (DWBA) analysis [26]. The data suggest an increase from $N = 140-142$. The (p,t) intensities produced by the *sdf*-IBM exhibit a similar trend. As in the case of the Ra chain, the *sd*-

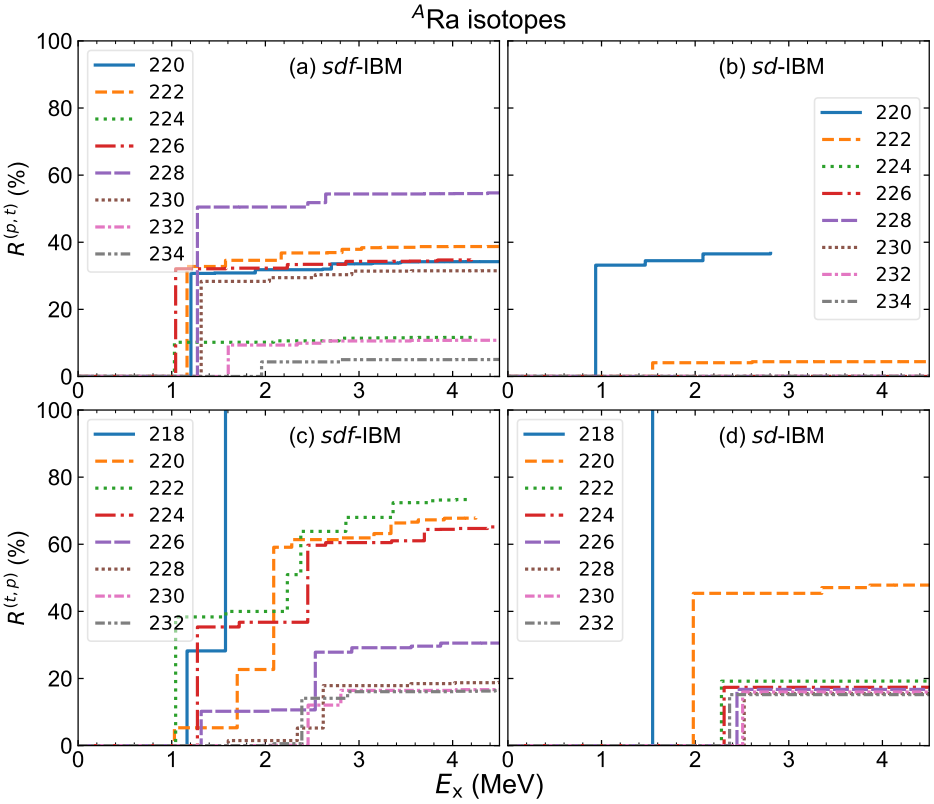

FIG. 10. Running sums, $R^{(p,t)}$ and $R^{(t,p)}$, for $^{A+2}$Ra$(p,t)^A$Ra and ^{A}Ra$(t,p)^{A+2}$Ra reactions with $A = 218 - 232$, respectively. Results from the *sdf*-IBM [(a) and (c)] and *sd*-IBM [(b) and (d)] are compared.

IBM suggests a monotonous, weak N dependence of the $I^{(p,t)}(0_1^+ \to 0_1^+)$ and $I^{(t,p)}(0_1^+ \to 0_1^+)$ values, except for the lightest Th nuclei.

The predicted $I^{(p,t)}(0_1^+ \to 0_2^+)$ and $I^{(t,p)}(0_1^+ \to 0_2^+)$ intensities for Th in the *sdf*-IBM exhibit peaks at $N = 140$ and $N = 134$, respectively, and these behaviors are similar to those obtained for the Ra isotopes. The experimental cross sections for the (p,t) transfers [26] indicates an increasing pattern from $N = 140 - 142$. The present *sdf*-IBM values of $I^{(p,t)}(0_1^+ \to 0_2^+)$, however, decrease from $N = 140$ to 146.

To infer gross features of the (p,t) and (t,p) strengths to excited 0^+ states, running sums of the relative transfer intensities

$$R^\alpha = \sum_{n=2} \frac{I^\alpha(0_1^+ \to 0_n^+)}{I^\alpha(0_1^+ \to 0_1^+)} \,, \tag{15}$$

with $\alpha = (p,t)$ or (t,p), normalized with respect to the transfer strength to the ground state, are considered. Figures 10 and 11 give the corresponding results for Ra and Th isotopes, respectively. It is seen from Fig. 10(a) that, for all Ra isotopes, the $0_1^+ \to 0_2^+$ transfers dominate the (p,t) strengths to the excited 0^+ states in the considered energy range of $E_x \leqslant 4.5$ MeV in the *sdf*-IBM: The sums, $R^{(p,t)}$, converge at the 0_2^+ excitation energies, which are typically $1 \sim 1.5$ MeV. For the ^{232}Ra$(p,t)^{230}$Ra and ^{234}Ra$(p,t)^{232}$Ra (p,t) reactions, the running sums amount to $R^{(p,t)} \approx 10$ %, and thus transfer strengths to the excited 0^+ states are of minor importance. The *sdf*-IBM suggests that the $R^{(p,t)}$ sums for the ^{228}Ra$(p,t)^{226}$Ra and ^{224}Ra$(p,t)^{222}$Ra reactions converge to particularly high (≈ 50 %) and low (≈ 10 %) values, respectively, as compared with those for the (p,t) reactions of neighboring isotopes. The peculiar tendencies are expected from the behaviors of the $I^{(p,t)}(0_1^+ \to 0_2^+)$ values, being small at $N = 136$ and maximal at $N = 140$ [see, Fig. 8(c)], which reflect, to a large extent, the octupole correlation effects. In the *sd*-IBM, there is essentially no contribution from the (p,t) transfers to excited 0^+ states, except for the ^{220}Ra$(p,t)^{218}$Ra and ^{222}Ra$(p,t)^{220}$Ra reactions.

As one sees in Fig. 10(c), the running (t,p) strengths continue to increase with E_x. In majority of the cases, there appear two major rises of the running sums, one at the 0_2^+ excitation energies and the other at $E_x \approx 2 \sim 3$ MeV. The sums appear to converge at $E_x > 3$ MeV. Only for the ^{218}Ra$(t,p)^{220}$Ra reaction, the sum exceeds the $I^{(t,p)}(0_1^+ \to 0_1^+)$ intensity at the excitation energy of the 0_3^+ state in ^{220}Ra. The $R^{(t,p)}$ values for ^{220}Ra$(t,p)^{222}$Ra, ^{222}Ra$(t,p)^{224}$Ra, ^{224}Ra$(t,p)^{226}$Ra reactions reach more than 60 % at $E_x > 2$ MeV. For those (t,p) transfers of the

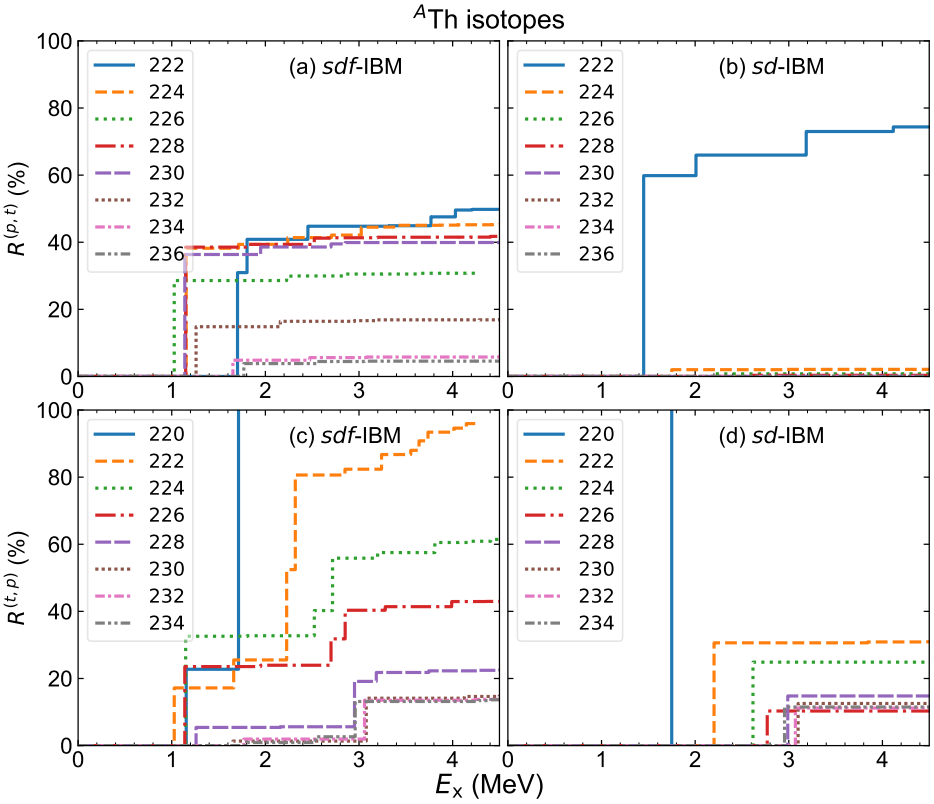

FIG. 11. Same as the caption to Fig. 10, but for the $^{A+2}$Th$(p,t)^A$Th and ^{A}Th$(t,p)^{A+2}$Th reactions with $A = 220 - 234$.

Ra nuclei with mass $A \geqslant 228$, contributions of the $0_1^+ \to 0_{\rm ex}^+$ transfers become less significant in comparison with the $0_1^+ \to 0_1^+$ ones. These results are expected from the systematic behaviors of the $I^{(t,p)}(0_1^+ \to 0_{1,2}^+)$ intensities, shown in Figs. 8(b) and 8(d). In the *sd*-IBM, the (t,p) running sums, $R^{(t,p)}$, shown in Fig. 10(d), are almost purely accounted for by the $0_1^+ \to 0_2^+$ transfer, while there is no contribution from the transfer strengths to higher-lying 0^+ states.

Figure 11 gives the running sums calculated for the Th isotopes. Similarly to the Ra case, the *sdf*-IBM suggests that the $0_1^+ \to 0_2^+$ transfers are most important among the $0_1^+ \to 0_{\rm ex}^+$ strengths, with the running sums being converged approximately at the 0_2^+ energies, and that contributions from the transfer strengths to higher-lying 0^+ states are only incremental. The $R^{(p,t)}$ values become smaller for transfer reactions of heavier Th isotopes. However, the converged $R^{(p,t)}$ values for the ^{228}Th$(p,t)^{226}$Th and ^{230}Th$(p,t)^{228}$Th reactions are larger than that of the ^{226}Th$(p,t)^{224}$Th one. This irregularity arises from the large $I^{(p,t)}(0_1^+ \to 0_2^+)$ values calculated for the (p,t) transfers of ^{228}Th and ^{230}Th, as compared with those of other nuclei; see Fig. 9(c).

One can compare the mapped *sdf*-IBM running sums with the experimental counterparts for the ^{230}Th$(p,t)^{228}$Th [28] and ^{232}Th$(p,t)^{230}$Th [27] reactions. In Refs. [27, 28], phenomenological *spdf*-IBM and quasiparticle-phonon model (QPM) calculations were also performed. It was shown in Ref. [27] that the measured running sum for the relative ^{232}Th$(p,t)^{230}$Th transfer intensity exhibited a significant rise at the 0_2^+ excitation energy in ^{230}Th to amount to $R^{(p,t)} \approx 30$ %, and a second rise in the range $E_x \approx 1.5 \sim 2.5$, increasing from 30 % ($E_x \approx 1.5$ MeV) to 60 % ($E_x \approx 2.5$ MeV). Both the *spdf*-IBM and QPM reproduced this trend. The (p,t) relative running sum predicted by the *sdf*-IBM for ^{232}Th$(p,t)^{230}$Th exhibits only a single rise at the 0_2^+ state in ^{230}Th, and converges to $R^{(p,t)} \approx 40$ %. The experimental running sum for the ^{230}Th$(p,t)^{228}$Th transfer was shown [28] to be rather stable at ≈ 20 % from $E_x \approx 0.6$ MeV, corresponding to the 0_2^+ excitation energy, to $E_x \approx 1.5$ MeV, but exhibit a second, steady rise for $E_x > 1.5$ MeV. The QPM calculation in Ref. [28] qualitatively reproduced this trend. In the present *sdf*-IBM, the relative running sum for the ^{230}Th$(p,t)^{228}$Th reaction reaches $R^{(t,p)} \approx 20$ %, but exhibits only a single rise at the 0_2^+ excitation energy.

Systematic of the (t,p) running sums in Th isotopes, shown in Fig. 11(c), appears to be similar to that of Ra isotopes, that is, the converged values of the running sum become smaller for the (t,p) transfers of heavier isotopes, and a second rise of the sums appears within the energy

range of $E_x \approx 2.5 \sim 3$ MeV. The results obtained from the *sd*-IBM, shown in Figs. 11(b), and 11(d) are also quite similar to those for the Ra isotopes.

IV. CONCLUSIONS

Octupole correlation effects on the excited 0^+ states and two-neutron transfer intensities in actinide nuclei have been investigated in the framework of the *sdf*-IBM, using the interaction strength parameters determined by means of the microscopic SCMF method. The calculated energy levels of the 0_2^+ states in the *sdf*-IBM for most of the considered nuclei were shown to be significantly lower and closer to experimental values than those of the *sd*-IBM. The *sdf*-IBM also turned out to give an improved description of the positive-parity even-spin yrast states in the ground-state bands. The *sdf*-IBM produces a large number of excited 0^+ states, most of which are composed of the configurations containing more than one f bosons.

Octupole correlations have been shown to have significant influences on two-neutron transfer intensities in actinide nuclei. For the $0_1^+ \to 0_2^+$ (p,t) and (t,p) transfer intensities, contributions from the f-boson term in the transfer operators turned out to be larger than those from the leading-order, s-boson term, particularly for those nuclei with $N = 132 - 138$, in which enhanced octupole collectivity is expected. Furthermore, the mapped *sdf*-IBM predicts some characteristic behaviors of the (p,t) and (t,p) intensities for the $0_1^+ \to 0_{1,2}^+$ transitions as functions of N along each isotopic chain, which can be regarded as signatures of the possible shape phase transitions. The *sd*-IBM, however, gives monotonous evolution with N of these transfer intensities.

The octupole degree of freedom appears to be relevant to the mapped IBM description of the low-lying states of both parity and two-nucleon transfers in the actinide region. The results shed lights upon the interpretation of the low-energy 0_2^+ states and corresponding bands observed in light actinides in terms of the double-octupole-phonon structure. The overestimates of the 0_2^+ energy levels, which still persist in some Ra and Th nuclei with $N \geqslant 138$, may indicate yet another correlations that are missing in the present version of the theoretical framework, e.g., configuration mixing. These points will be addressed as a future study and reported elsewhere.

ACKNOWLEDGMENTS

This work has been supported by JSPS KAKENHI Grant No. JP25K07293.

[1] A. Bohr and B. R. Mottelson, *Nuclear Structure*, Vol. II (Benjamin, New York, USA, 1975).
[2] I. Ahmad and P. A. Butler, Annu. Rev. Nucl. Part. Sci. **43**, 71 (1993).
[3] P. A. Butler and W. Nazarewicz, Rev. Mod. Phys. **68**, 349 (1996).
[4] P. A. Butler, J. Phys. G: Nucl. Part. Phys. **43**, 073002 (2016).
[5] P. A. Butler, Proc. R. Soc. A **476**, 20200202 (2020).
[6] P. A. Butler, Phys. Scr. **99**, 035302 (2024).
[7] L. P. Gaffney, P. A. Butler, M. Scheck, A. B. Hayes, F. Wenander, M. Albers, B. Bastin, C. Bauer, A. Blazhev, S. Bönig, N. Bree, J. Cederkäll, T. Chupp, D. Cline, T. E. Cocolios, T. Davinson, H. D. Witte, J. Diriken, T. Grahn, A. Herzan, M. Huyse, D. G. Jenkins, D. T. Joss, N. Kesteloot, J. Konki, M. Kowalczyk, T. Kröll, E. Kwan, R. Lutter, K. Moschner, P. Napiorkowski, J. Pakarinen, M. Pfeiffer, D. Radeck, P. Reiter, K. Reynders, S. V. Rigby, L. M. Robledo, M. Rudigier, S. Sambi, M. Seidlitz, B. Siebeck, T. Stora, P. Thoele, P. V. Duppen, M. J. Vermeulen, M. von Schmid, D. Voulot, N. Warr, K. Wimmer, K. Wrzosek-Lipska, C. Y. Wu, and M. Zielinska, Nature (London) **497**, 199 (2013).
[8] K. Heyde, P. Van Isacker, M. Waroquier, J. L. Wood, and R. A. Meyer, Phys. Rep. **102**, 291 (1983).
[9] J. L. Wood, K. Heyde, W. Nazarewicz, M. Huyse, and P. van Duppen, Phys. Rep. **215**, 101 (1992).
[10] K. Heyde and J. L. Wood, Rev. Mod. Phys. **83**, 1467 (2011).
[11] P. E. Garrett, M. Zielińska, and E. Clément, Prog. Part. Nucl. Phys. **124**, 103931 (2022).
[12] S. Leoni, B. Fornal, A. Bracco, Y. Tsunoda, and T. Otsuka, Prog. Part. Nucl. Phys. **139**, 104119 (2024).
[13] L. Carr, ed., *Understanding Quantum Phase Transitions* (CRC Press, 2010).
[14] R. F. Casten, Prog. Part. Nucl. Phys. **62**, 183 (2009).
[15] P. Cejnar, J. Jolie, and R. F. Casten, Rev. Mod. Phys. **82**, 2155 (2010).
[16] L. Fortunato, Prog. Part. Nucl. Phys. **121**, 103891 (2021).
[17] D. Bès and R. Broglia, Nucl. Phys. **80**, 289 (1966).
[18] D. Bès, R. Broglia, and B. Nilsson, Phys. Lett. B **40**, 338 (1972).
[19] R. A. Broglia, O. Hansen, and C. Riedel, Two-neutron transfer reactions and the pairing model, in *Advances in Nuclear Physics: Volume 6*, edited by M. Baranger and E. Vogt (Springer US, Boston, MA, 1973) pp. 287–457.
[20] L. Próchniak, K. Zając, K. Pomorski, S. Rohoziński, and J. Srebrny, Nucl. Phys. A **648**, 181 (1999).
[21] D. M. Brink and R. A. Broglia, *Nuclear superfluidity: pairing in finite systems* (Cambridge University Press, 2005).
[22] J. Srebrny, T. Czosnyka, C. Droste, S. G. Rohoziński, L. Próchniak, K. Zając, K. Pomorski, D. Cline, C. Y. Wu, A. Bäcklin, L. Hasselgren, R. M. Diamond, D. Habs, H. J. Körner, F. S. Stephens, C. Baktash, and R. P. Kostecki, Nucl. Phys. A **766**, 25 (2006).
[23] L. Próchniak, Int. J. Mod. Phys. E **16**, 352 (2007).
[24] J. Xiang, Z. P. Li, T. Nikšić, D. Vretenar, and W. H. Long, Phys. Rev. C **101**, 064301 (2020).

[25] K. Nomura, D. Vretenar, Z. P. Li, and J. Xiang, Phys. Rev. C **102**, 054313 (2020).
[26] H.-F. Wirth, G. Graw, S. Christen, D. Cutoiu, Y. Eisermann, C. Günther, R. Hertenberger, J. Jolie, A. I. Levon, O. Möller, G. Thiamova, P. Thirolf, D. Tonev, and N. V. Zamfir, Phys. Rev. C **69**, 044310 (2004).
[27] A. I. Levon, G. Graw, Y. Eisermann, R. Hertenberger, J. Jolie, N. Y. Shirikova, A. E. Stuchbery, A. V. Sushkov, P. G. Thirolf, H.-F. Wirth, and N. V. Zamfir, Phys. Rev. C **79**, 014318 (2009).
[28] A. I. Levon, G. Graw, R. Hertenberger, S. Pascu, P. G. Thirolf, H.-F. Wirth, and P. Alexa, Phys. Rev. C **88**, 014310 (2013).
[29] M. Spieker, D. Bucurescu, J. Endres, T. Faestermann, R. Hertenberger, S. Pascu, S. Skalacki, S. Weber, H.-F. Wirth, N.-V. Zamfir, and A. Zilges, Phys. Rev. C **88**, 041303 (2013).
[30] M. Spieker, S. Pascu, D. Bucurescu, T. M. Shneidman, T. Faestermann, R. Hertenberger, H.-F. Wirth, N.-V. Zamfir, and A. Zilges, Phys. Rev. C **97**, 064319 (2018).
[31] N. V. Zamfir, J.-y. Zhang, and R. F. Casten, Phys. Rev. C **66**, 057303 (2002).
[32] D. A. Meyer, V. Wood, R. F. Casten, C. R. Fitzpatrick, G. Graw, D. Bucurescu, J. Jolie, P. v. Brentano, R. Hertenberger, H.-F. Wirth, N. Braun, T. Faestermann, S. Heinze, J. L. Jerke, R. Krücken, M. Mahgoub, O. Möller, D. Mücher, and C. Scholl, Phys. Rev. C **74**, 044309 (2006).
[33] S. Pascu, G. Căta-Danil, D. Bucurescu, N. Mărginean, N. V. Zamfir, G. Graw, A. Gollwitzer, D. Hofer, and B. D. Valnion, Phys. Rev. C **79**, 064323 (2009).
[34] S. Pascu, G. Căta-Danil, D. Bucurescu, N. Mărginean, C. Müller, N. V. Zamfir, G. Graw, A. Gollwitzer, D. Hofer, and B. D. Valnion, Phys. Rev. C **81**, 014304 (2010).
[35] D. Bucurescu, S. Pascu, G. Suliman, H.-F. Wirth, R. Hertenberger, T. Faestermann, R. Krücken, and G. Graw, Phys. Rev. C **100**, 044316 (2019).
[36] A. I. Levon, D. Bucurescu, C. Costache, T. Faestermann, R. Hertenberger, A. Ionescu, R. Lica, A. G. Magner, C. Mihai, R. Mihai, C. R. Nita, S. Pascu, K. P. Shevchenko, A. A. Shevchuk, A. Turturica, and H.-F. Wirth, Phys. Rev. C **102**, 014308 (2020).
[37] F. Iachello and A. Arima, *The interacting boson model* (Cambridge University Press, Cambridge, 1987).
[38] A. Arima and F. Iachello, Phys. Rev. C **16**, 2085 (1977).
[39] R. Fossion, C. E. Alonso, J. M. Arias, L. Fortunato, and A. Vitturi, Phys. Rev. C **76**, 014316 (2007).
[40] Y. Zhang and F. Iachello, Phys. Rev. C **95**, 034306 (2017).
[41] K. Nomura and Y. Zhang, Phys. Rev. C **99**, 024324 (2019).
[42] J. García-Ramos, J. Arias, and A. Vitturi, Chin. Phys. C **44**, 124101 (2020).
[43] K. Nomura, Phys. Rev. C **113**, 044318 (2026).
[44] P. Ring and P. Schuck, *The Nuclear Many-Body Problem* (Springer-Verlag, Berlin, 1980).
[45] M. Bender, P.-H. Heenen, and P.-G. Reinhard, Rev. Mod. Phys. **75**, 121 (2003).
[46] D. Vretenar, A. V. Afanasjev, G. A. Lalazissis, and P. Ring, Phys. Rep. **409**, 101 (2005).
[47] L. M. Robledo, T. R. Rodríguez, and R. R. Rodríguez-Guzmán, J. Phys. G: Nucl. Part. Phys. **46**, 013001 (2019).
[48] K. Nomura, Eur. Phys. J. A **61**, 139 (2025).
[49] K. Nomura, D. Vretenar, and B.-N. Lu, Phys. Rev. C **88**, 021303 (2013).
[50] K. Nomura, D. Vretenar, T. Nikšić, and B.-N. Lu, Phys. Rev. C **89**, 024312 (2014).
[51] K. Nomura, R. Rodríguez-Guzmán, Y. M. Humadi, L. M. Robledo, and J. E. García-Ramos, Phys. Rev. C **102**, 064326 (2020).
[52] S. Goriely, S. Hilaire, M. Girod, and S. Péru, Phys. Rev. Lett. **102**, 242501 (2009).
[53] J. Decharge, M. Girod, and D. Gogny, Phys. Lett. B **55**, 361 (1975).
[54] O. Scholten, F. Iachello, and A. Arima, Ann. Phys. (NY) **115**, 325 (1978).
[55] J. Engel and F. Iachello, Phys. Rev. Lett. **54**, 1126 (1985).
[56] J. Engel and F. Iachello, Nucl. Phys. A **472**, 61 (1987).
[57] A. F. Barfield, B. R. Barrett, J. L. Wood, and O. Scholten, Ann. Phys. **182**, 344 (1988).
[58] T. Otsuka, A. Arima, F. Iachello, and I. Talmi, Phys. Lett. B **76**, 139 (1978).
[59] T. Otsuka, A. Arima, and F. Iachello, Nucl. Phys. A **309**, 1 (1978).
[60] K. Nomura, R. Rodríguez-Guzmán, and L. M. Robledo, Phys. Rev. C **92**, 014312 (2015).
[61] K. Nomura, N. Shimizu, and T. Otsuka, Phys. Rev. Lett. **101**, 142501 (2008).
[62] K. Nomura, T. Otsuka, N. Shimizu, and L. Guo, Phys. Rev. C **83**, 041302 (2011).
[63] H. Schaaser and D. Brink, Nucl. Phys. A **452**, 1 (1986).
[64] D. J. Thouless and J. G. Valatin, Nucl. Phys. **31**, 211 (1962).
[65] K. Nomura, Phys. Rev. C **106**, 024330 (2022).
[66] Brookhaven National Nuclear Data Center, `http://www.nndc.bnl.gov`.
[67] P. A. Butler, L. P. Gaffney, P. Spagnoletti, K. Abrahams, M. Bowry, J. Cederkäll, G. de Angelis, H. De Witte, P. E. Garrett, A. Goldkuhle, C. Henrich, A. Illana, K. Johnston, D. T. Joss, J. M. Keatings, N. A. Kelly, M. Komorowska, J. Konki, T. Kröll, M. Lozano, B. S. Nara Singh, D. O'Donnell, J. Ojala, R. D. Page, L. G. Pedersen, C. Raison, P. Reiter, J. A. Rodriguez, D. Rosiak, S. Rothe, M. Scheck, M. Seidlitz, T. M. Shneidman, B. Siebeck, J. Sinclair, J. F. Smith, M. Stryjczyk, P. Van Duppen, S. Vinals, V. Virtanen, N. Warr, K. Wrzosek-Lipska, and M. Zielińska, Phys. Rev. Lett. **124**, 042503 (2020).
[68] H. Wollersheim, H. Emling, H. Grein, R. Kulessa, R. Simon, C. Fleischmann, J. de Boer, E. Hauber, C. Lauterbach, C. Schandera, P. Butler, and T. Czosnyka, Nucl. Phys. A **556**, 261 (1993).
[69] F. K. McGowan, C. E. Bemis, W. T. Milner, J. L. C. Ford, R. L. Robinson, and P. H. Stelson, Phys. Rev. C **10**, 1146 (1974).
[70] F. McGowan and W. Milner, Nucl. Phys. A **562**, 241 (1993).
[71] P. D. Duval and B. R. Barrett, Phys. Lett. B **100**, 223 (1981).
[72] K. Nomura, R. Rodríguez-Guzmán, L. M. Robledo, and N. Shimizu, Phys. Rev. C **86**, 034322 (2012).
[73] K. Nomura, T. Otsuka, and P. Van Isacker, J. Phys. G: Nucl. Part. Phys. **43**, 024008 (2016).
[74] P. E. Garrett, W. D. Kulp, J. L. Wood, D. Bandyopadhyay, S. Choudry, D. Dashdorj, S. R. Lesher, M. T. McEl-

listrem, M. Mynk, J. N. Orce, and S. W. Yates, Phys. Rev. Lett. **103**, 062501 (2009).
[75] Y. Tsunoda, N. Shimizu, and T. Otsuka, Phys. Rev. C **108**, L021302 (2023).
[76] K. Nomura, Phys. Lett. B **871**, 139995 (2025).